



# City Research Online

## City St George's, University of London

**Citation:** Kovacevic, A. (2017). Algebraic generation of single domain computational grid for twin screw machines. Part I. Implementation. *Advances in Engineering Software*, 107, pp. 38-50. doi: 10.1016/j.advengsoft.2017.02.003

This is the accepted version of the paper.

This version of the publication may differ from the final published version. To cite this item please consult the publisher's version.

**Permanent repository link:** <https://openaccess.city.ac.uk/id/eprint/16955/>

**Link to published version:** <https://doi.org/10.1016/j.advengsoft.2017.02.003>

**Copyright and Reuse:** Copyright and Moral Rights remain with the author(s) and/or copyright holders. Copies of full items can be used for personal research or study, educational, or not-for-profit purposes without prior permission or charge, unless otherwise indicated, provided that the authors, title and full bibliographic details are credited, a hyperlink and/or URL is given for the original metadata page and the content is not changed in any way. For full details of reuse please refer to [City Research Online policy](#).

## **Algebraic Generation of Single Domain Computational Grid for Twin Screw Machines**

### **Part I – Implementation**

Sham Rane\*, Ahmed Kovacevic

Centre for Compressor Technology, City, University of London, EC1V 0HB, London, U.K.

Email: [sham.rane@city.ac.uk](mailto:sham.rane@city.ac.uk) , Tel: +44(0) 20 70408795,

\* Corresponding Author

#### **Abstract**

Special attention is required for generation of computational grids in highly deforming working chambers of twin screw machines for 3D CFD calculations. Two approaches for customised grid generation are practically available. The first is an algebraic grid generation and the second is a differential decomposition method. This paper reports on new developments in the algebraic approach that has the advantages associated with both algebraic and differential methods. Two control functions are introduced for regularisation of the initial algebraic distribution. One is based on an analytical control function in transformed coordinate system while the other uses background blocking structure in order to guide the initial algebraic distribution towards a single computational mesh. This paper presents implementation and grid characteristics of these new functions. Developed grids have been tested and results from flow calculations on a dry air compressor have been validated in part II [29] of the paper.

It was possible to achieve two distinct characteristics desirable in a twin screw rotor domain mesh. Firstly, it is possible to independently control grid refinement in the interlobe region thereby providing better accuracy in representation of the leakage gaps. Secondly and most importantly, it is possible now to eliminate the non-conformal interface between the two rotor domains thereby producing a single domain structured grid for the rotors, while still maintaining the fully hexahedral cell topology. An improvement in the global orthogonality of the cells was achieved. Despite of a decrement in the Face warp quality, aspect ratio of cells retained similar scale.

#### **Keywords**

Computational Fluid Dynamics, Algebraic Grid Generation, Twin Screw Compressors, Deforming Grid, Positive Displacement Compressors.

#### **Nomenclature**

$A_{sk}$	- amplitude of the sine function	$x, y$	- Cartesian coordinates
$n_{sk}$	- frequency of the sine function	$r, \theta$	- polar coordinates of a point
$\sigma_{sk}$	- skewness of the sine function	$\xi, \eta$	- Computational coordinates

$t$	- period of the sine function	$S_i$	- arc-length increment
$t_i$	- time scale at a boundary node	$S_I$	- length of the boundary
$\phi_w$	- wrap angle	$\mathbf{n}$	- cell face normal vector
$z_1$	- Number of lobes on main rotor	$\mathbf{rb}(x, y)$	- Blocking node position vector
$z_2$	- Number of lobes on gate rotor	$\mathbf{B}_i$	- Blocking index
$i_{casing}$	- node count on the casing curve	$\mathbf{r}$	- radius vector
$i_{rack}$	- node count on the rack curve	$Q_{min}$	- smallest angle in an element
$r_o$	- radius of the rotor	$Q_{max}$	- largest angle in an element
$r_{oc}$	- radius of the outer circle	$Q_e$	- equiangular element = $90^\circ$

### Abbreviations

ALE	- Arbitrary Lagrangian-Eulerian	TFI	- Transfinite Interpolation
SCORG	- Screw Compressor Rotor Grid Generator	GGI	- Generalised Grid Interface
RC	- Distribution from Rotor boundary to the Casing boundary	CR	- Distribution from Casing boundary to the Rotor boundary

## 1 Introduction

Early reports on the application of CFD in analysis of screw machines can be found in *Stošić, Smith and Zagorac* (1996) [22]. They presented a solution in positive displacement compressor of screw and scroll type geometry without full grid deformation but by the addition of a representative momentum source. The results were encouraging for pressure distribution but did not show realistic flow properties. A breakthrough was achieved in 1999 by *Kovačević* [9] with the use of a numerical rack generation method to generate an algebraic, adaptive, block structured, deforming numerical grid for screw compressors when the full 3D transient CFD calculation of twin screw compressor was performed for the first time. Since then there have been several activities reported on the CFD analysis of screw machines. The analysis of the screw compressor working chamber is transient in nature and requires a grid to represent each rotor position during the flow calculation. Algebraic grid generation methods are fast and robust. An alternative approach in *Vande Voorde* (2005) [26] uses differential domain decomposition and grid manipulation to generate numerical mesh for screw rotor domains. Differential methods are much slower than algebraic ones but have shown some advantages in achieving better orthogonality and smoothness of the rotor mesh. This section gives detailed description and comparison of these two methods used for grid generation of a numerical mesh for screw machines.

### 1.1 Algebraic generation of twin screw rotor numerical grid

*Kovačević et al.* (2000) [8] pioneered in grid generation for screw rotors with algebraic method that features boundary adaptation and transfinite interpolation. It is implemented in the computer code called SCORG (Screw Compressor Rotor Grid Generation) in which the basic grid generation algorithm is written in FORTRAN with a C# and Microsoft .Net front end graphical user interface. In his thesis, *Kovačević* (2002) [9] presented these aspects of grid generation in detail. *Kovačević et al.* (2002, 2005 and 2007) [9, 10, 11] have reported CFD simulations of twin screw machines to predict gas flow, conjugate heat transfer, fluid-structure interaction etc. for variety of screw machines. The domain of a screw machines is commonly decomposed into the low pressure port domain, the rotor domain and the high pressure port domain. A block structured numerical mesh is required in the stretching and sliding rotor domain in order to preserve conservativeness of the solution. The rotor grid is generated in the O form which requires a flow domain between rotors and the casing to be divided in two blocks each belonging to one of the rotors. One O grid is constructed on the side of the male rotor and other on the female side. The division is achieved by use of rack – the rotor with infinite radius which uniquely exists between two rotors. It is generated by use of envelope method of gearing as explained *Kovačević et al.* (2007) [11]. The rack and outer casing circles are connected in the cross section of the rotor domain to split it into two O grid domains as shown in Figure 1a. Boundary nodes are first positioned on the rotor boundaries using adaptation functions described in *Kovačević* (2005) [10] as shown in Figure 1b. These nodes retain relative position to the rotor and rotate together with the rotor. The boundary nodes on the outer boundary which consists of the casing circle and the rack are distributed using boundary distribution method described in *Kovačević* (2005) [10]. These nodes slide on the outer boundary as the rotor rotates. Such a grid is being referred to as Rotor to Casing grid or “RC grid”. In essence, each of the O grid block rotates and deforms. The two O grids used in this method slide relative to each other. *Rane et al.* (2013 and 2014) [14, 15] recently extended the use of RC grid to generate deforming grids for variable geometry rotors with both variable lead and variable profile.

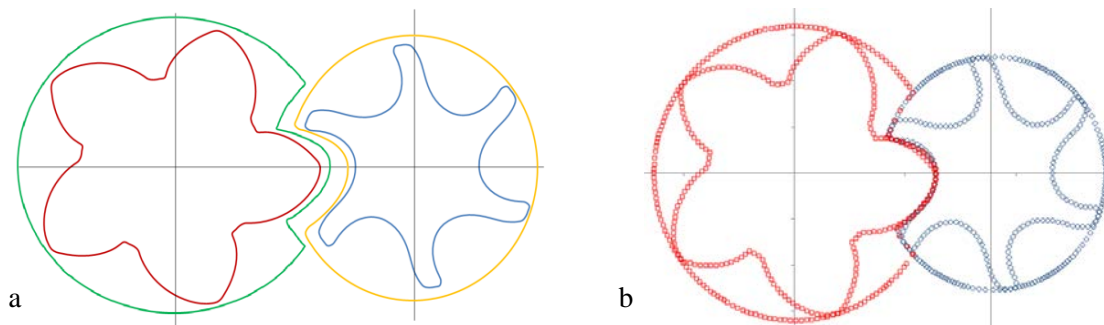


Figure 1 Decomposition of the rotor domain in algebraic rotor grid

a) O Grid boundaries, b) Discretised boundaries

The mentioned method for generating RC algebraic grids is fast and robust but introduces two grid features which require further attention namely, a non-conformal interface between the O grids and degenerated hexahedral numerical cells in the CUSP. Both of these are problematic for some CFD solvers as these cannot handle them conservatively. The objective of the work presented in this paper is to improve the grid generation method in order to resolve limitations caused by these undesired features of the RC type mesh.

### 1.1.1 Non-Conformal interface between blocks of RC grid.

Figure 2 shows an example of a non-conformal interface between the two rotor blocks of a RC type grid. Such grids offer good quality cells in terms of orthogonality and aspect ratio which could be independently controlled by boundary distribution and adaptation as well as orthogonalisation and smoothing of the TFI grid as explained in Kovacevic et al (2007) [11]. But the presence of a non-conformal interface raises concerns about the conservativeness of the flux balance that will be achieved across the interface between two blocks and the stability of a solver in case of multiphase calculation with additional physical equations as in the case of liquid injection machines. Moreover not all solvers are capable of defining a robust interface with highly deforming, stretching and sliding interface as in a helical screw machines. The desired option is to generate a conformal interface in which the nodes will correspond in both domains or if possible to eliminate the interface completely and generate a single mesh block.

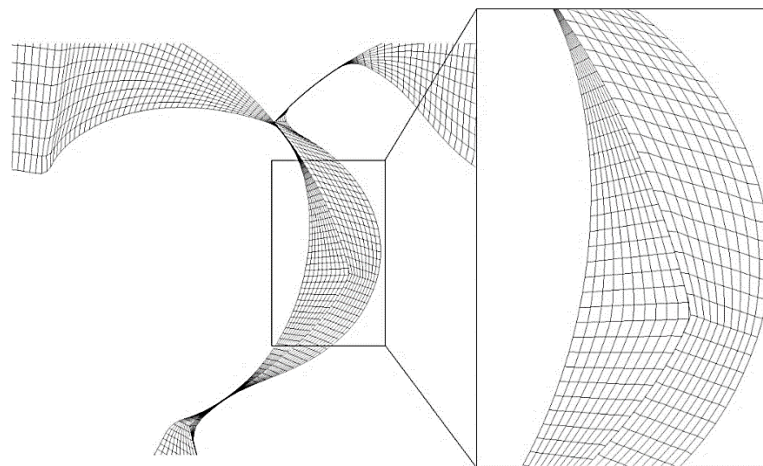


Figure 2 Non-conformal interface between the two rotors of RC type grid

### 1.1.2 Degenerated hexahedral numerical cells in the CUSP

In a RC type grid, the rotor boundary is mapped with computational nodes fixed to the rotor while the nodes on the casing are sliding to follow the movement of the rotor. In order to preserve a CUSP line

between the rotor bores in the axial direction which is required for accurate geometric representation of the blow-hole area, each numerical cell which slides on the casing boundary need to pass through the single point in the CUSP as shown in Figure 3. This is achieved by collapsing two neighbouring vertices of the boundary cell which results in creation of a cell with prism topology around the CUSP point. The cells still retain hexahedral definition with 8 vertices but some of these are simply occupying the same position in space. By this means the conservation of space is fully achieved but in some solvers, due to their internal node merging procedure, it results in degenerated numerical cells. Hence it is desirable to produce a grid with fully hexahedral cells which will retain all eight vertices to have different position in space during deformation.

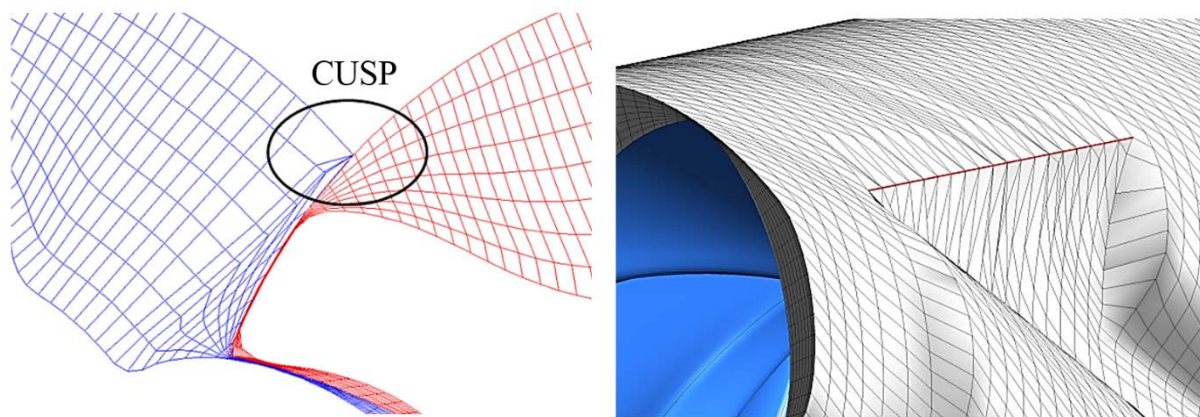


Figure 3 Nodes merged at the CUSP point to capture blow-hole area in a RC type grid

## 1.2 Differential generation for twin screw rotor numerical grid

Fundamentals of differential grid generation are presented in many works such as *Thompson, Thames and Mastin*, (1974) [23], *Soni*, (1992) [20], *Sorenson and Steger* (1977 and 1979) [19 21], *Shih et al.* (1991) [18], *Samareh and Smith*, (1992) [17]. In the field of screw compressor rotor grids, *Vande Voorde et al.* (2004 and 2005) [25, 26] were the first to implement a grid generation algorithm for block structured mesh from the solution of the Laplace equation. In his thesis, *Vande Voorde* (2005) [27] presented the principles of solving the initial Laplace equation and then using it to construct a block structured deforming mesh from the equipotential and gradient lines as shown in Figure 4a. Based on this grid generation, flow in a double tooth compressor and a twin screw compressor was analysed. *Papes et al.* (2014) [13] presented a 3D CFD analysis of twin screw expander using the grid generated by the differential grid generation approach. The differential equation based decomposition is a generic method that can be applied to a variety of twin rotor machines like lobe pumps, tooth compressors, screw compressors etc. With the differential approach, the rotor domain is treated as a number of 2D cross sections. Figure 4b shows the splitting curve or division line obtained in a 2D cross section of the compression chamber as an iso-potential line from the solution of  $\nabla^2\phi = 0$  with boundary conditions specified on the two rotors and the casing.

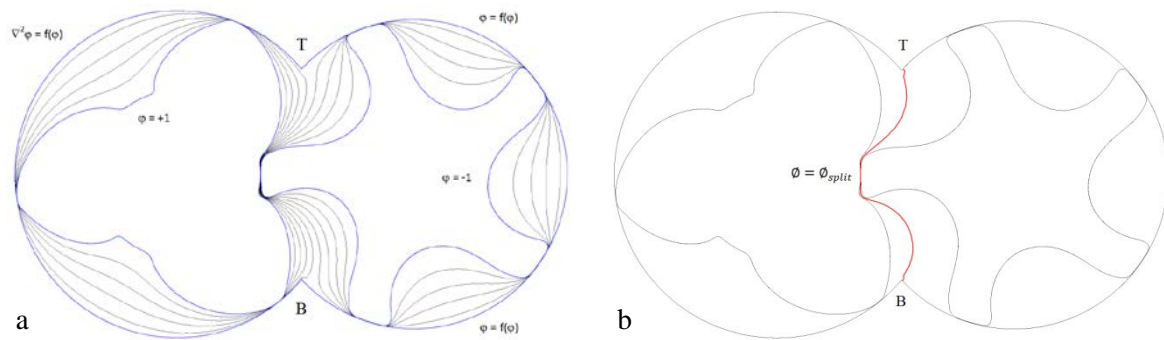


Figure 4 Solution of Laplace equation – a) Iso-potential lines and b) Splitting curve

A numerical scheme can be used to solve the Laplace equation in the 2D domain so formed (*Winslow, 1966 [28], Gordon and Hall, 1973 [6]*). Since the rotor profiles have close tolerances, the region formed between the casing and the two profiles has a very complex boundary. The distance between the rotor and the casing can vary from a few millimetres in the core region to a few micrometres in the clearance regions. Hence, discretisation, using unstructured triangular cells is the most appropriate. The gaps can be highly refined to capture the iso-potential lines conforming with the boundary, accurately. *Vande Voorde et al. (2005) [26]* used a customised Delaunay triangulation program (*Riemsloagh et al., 2000*) [16] for this initial triangular grid construction. In the final rotor grids, boundary nodes are first positioned on the casing and splitting curve. These nodes remain unchanged with respect to the rotor. The boundary nodes on the rotor are distributed with reference to the outer nodes. Rotor nodes slide on the profiles as the rotor rotates and cause warpage of the boundary cells on rotors with small radii in the profile as shown in Figure 5. Such a grid structure is referred to as Casing to Rotor grid type or in short CR type grid.

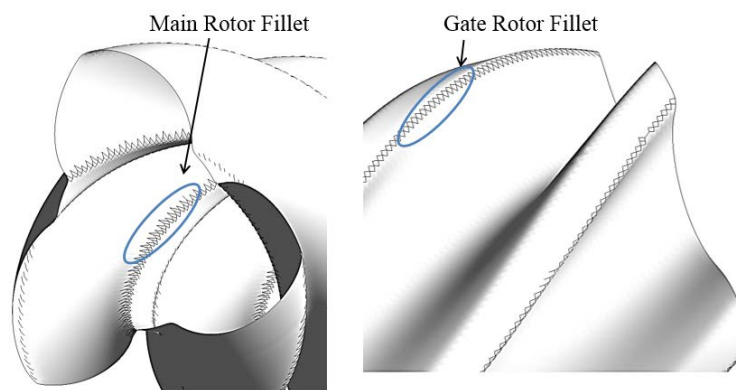


Figure 5 Warpage of faces at small radii on the two rotors of CR type grid

### 1.3 Comparison of the algebraic method RC grid and differential CR grid

Table 1 shows comparison of the grid generation methods used for analysis for screw machines. It is based on the features of the RC type grid generated using algebraic method from *Kovačević et al. (2002)* [9] and the CR type grid using hybrid differential method from *Vande Voorde et al. (2005)* [26].

Table 1 Comparison of algebraic and differential grid generation in twin screw compressors

Criteria	Algebraic Approach ( <i>Kovačević et al., 2002</i> ) [9]	Hybrid Differential Approach ( <i>Vande Voorde et al., 2005</i> ) [26]
1 Decomposition of the rotor domain	Analytical or Numerical rack. Rack based decomposition is very fast.	Division line is obtained by differential decomposition. Generic in nature but slow.
2 Grid type	Rotor $\Rightarrow$ Casing (RC type) The O blocks rotate with the rotor. Grid deformation occurs at the rack interface which is non-conformal. Rotor shape is fully preserved.	Casing $\Rightarrow$ Rotor (CR type) The O blocks are fixed to casing and do not rotate. Interface between domains is conformal. Rotor shape is deformed due to nodes sliding on its surface.
2 Boundary Distribution	Nodes are first distributed on the rotor boundary using selected adaptation criteria. Nodes on the casing are projected with regularity check.	Nodes are first distributed on Casing using equidistance and radius of curvature factors. Profile nodes are defined by projected gradient lines.
3 Interface between the two O Blocks	Non-Conformal. Non-Conformal interface is handled by flux balance in the solver, gives more flexibility for adaptation.	Conformal. Conformal interface gives higher solution accuracy. Demanded by some CFD solvers.
4 Speed of grid generation	A representative mesh with 50 rotor positions on an i3 processor takes 5 sec for boundary distribution and 30 sec for 2D mesh generation. To write the full set of 750 grids takes about 1 hour.	A representative mesh takes about 900 sec for one position on DS20 processor. Calculation of the full set of 50 rotor positions takes about 15 hours.
5 Cell structure	To retain the CUSP line, some cells are pyramid or prism cells due to merging of nodes at the CUSP.	All cells are purely hexahedral. Warp of the cells occurs on the rotor surface with small radii (female tip). This has effect on blow-hole area.
6 Adaptation to variable profile rotors	Possible with modification in the algorithm to execute 2D generation on each profile and with 3D grid rearrangement.	Practically challenging due to time requirement for potential solution in 3D or on multiple 2D profiles for each position.
7 Advantages	Fast and good control over the node distribution.	Fully Hexahedral smooth cells.

	Rotor profile smoothly captured grid. Grid refinement is easy to be achieved.	Conformal interface between O blocks makes the grid suitable for variety of solvers and complexities like Multiphase flows.
8	Difficulties Some solvers cannot handle non-conformal interface between the domains.	Computationally expensive and long grid generation procedure. Difficulty of handling profiles with very small radii in the profile shape.

As identified in Table 1, the differential method proposed by *Vande Voorde et al.* (2005) [26] has some advantages compared to algebraic method developed by authors. These are mainly due to the use of iso-potential lines to produce the mesh with fixed nodes on the casing and conformal interface between the O grids.

The objective of the work described in this paper is to develop an algebraic grid generation method for a single domain grid which will combine advantages of both algebraic methods speed and CR mesh convenience.

## 2 Algebraic generation for single domain grid of screw machines

By using a CR type grid it is possible to generate fully hexahedral cells and conformal interface between the O blocks by using algebraic method and achieve similar characteristics of the grid obtained by the differential approach but in much shorter time. However, the CR distribution using algebraic methods does not give reference to distribution of boundary points on rotors which was available in the differential approach through the iso-potential solution. Therefore, it is challenging to achieve a regular grid on rotors without any special treatments.

In the research presented here, the procedure for generating CR type mesh uses coordinate transformation. Additionally, two new procedures have been explored that complement the CR type grid and regularise the grid distribution on the rotors. The first approach uses coordinate transformation of the full rotor domain and a skewed sine function in the transformed domain adaptable for a given rotor profile. In the further text it is called Regularisation by analytical control functions and will be described in section 2.2. It is suitable for generating a conformal interface between the two O grids for straight rotor lobes. The second approach is based on the principle of background blocking as described in 2.3. In this case, a new distribution of rotor nodes in the CR type grid is guided by an initial distribution of nodes in the RC type grid. This approach makes it possible to independently refine the grid in the interlobe region in order to improve the quality of cells in the leakage gaps. By use of this approach a conformal interface between the two rotor O blocks could be achieved by placing a one to one node map on the splitting rack curve.

## 2.1 Coordinate transformations for generation of CR type grid

The main steps in generating the CR type grid are:

1. Split the rotor cross section into two O blocks using rack as the splitting curve (Figure 1a).
2. Define the outer boundary in each O block as a combination of the casing circle between the CUSPs around the rotor and rack between the rotors as shown in Figure 6.
3. Discretize the Casing part of the outer boundary using equidistant distribution.
4. Discretise the rack part of the outer boundary so that the same number of nodes is selected for both O blocks in order to maintain a conformal interface. This distribution does not need to be equidistant and could also be adapted based on the characteristics of rotor curves in the interlobe region. Figure 6 shows the distribution obtained on the outer boundaries of the two O blocks that will act as the reference for the rotor profile distribution.
5. Define inner boundary by the original points of the rotor profile.
6. Make coordinate transformation of the outer boundary and the inner boundary from the physical domain  $X^2$  with coordinates  $(x, y)$  to the computational domain  $\Xi^2$  with coordinates  $(\xi, \eta)$  as shown in Figure 7 and defined by equations 2 and 3.
7. Distribute nodes on the rotor profile with corresponding distribution available on the outer boundary. The initial distribution can be selected as the constant  $\xi$  coordinate intersections with the transformed rotor profile to get the  $\eta$  coordinate. But this will produce overlap in some regions, especially on the gate rotor as shown in Figure 8. This requires for this distribution to be regularised.
8. Regularise the rotor profile distribution. Two methods of regularisation have been presented in this paper and described in sections 2.2 and 2.3.
  - Analytical control function.
  - Background blocking distribution.
9. Reverse coordinate transformation from  $(\xi, \eta)$  to  $(x, y)$  domain to get the rotor geometry as defined by equation 5.
10. Produce numerical mesh using TFI (*Kovačević et al.*, 2002 [9], *Eiseman et al.* 1994 [3], *Kim and Thompson*, 1990 [7]).
11. Implement Orthogonalisation and Smoothing to improve the cell quality (*Kovačević et al.*, 2007 [11], *Chawner and Anderson*, 1991 [1], *Eiseman*, 1987 [2]).

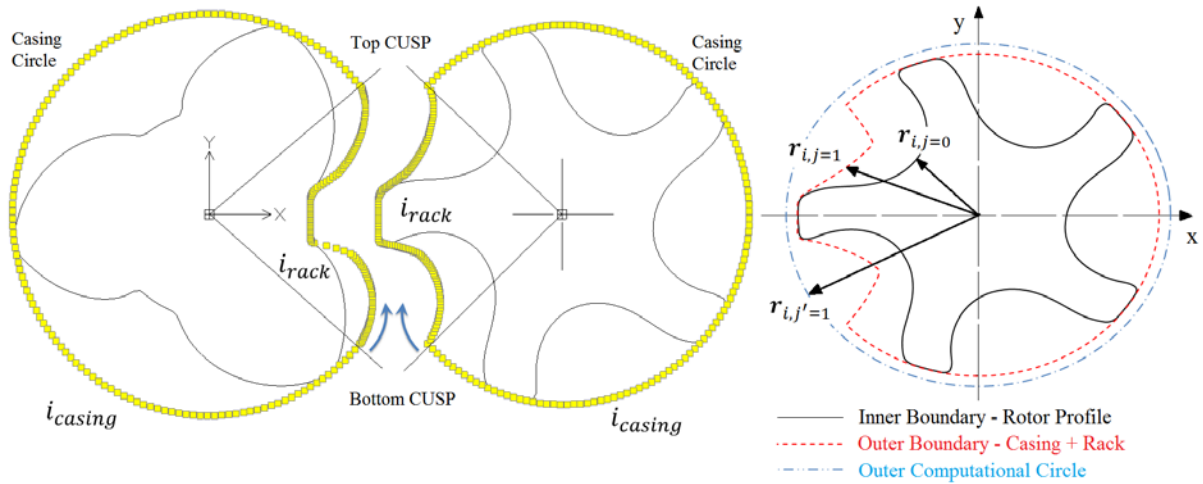


Figure 6 CR type grid point distribution of inner boundary and outer circle

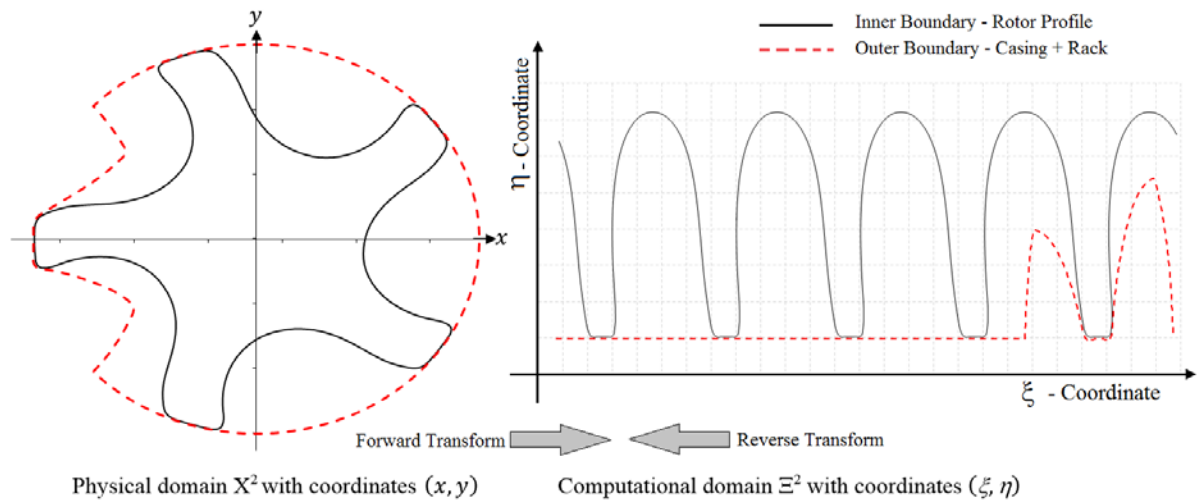


Figure 7 Physical and Computational domains with coordinate transformation of inner and outer boundary

The more detailed description of steps 3, 4, 5, 6 and 7 is given below.

A mapping function is used to transform the full inner and outer boundary from the physical to the computational domain. In the case of the RC type grid, this transformation needs to be performed only for one interlobe space since the distribution of the inner boundary remains unchanged for the entire rotor. However, for the CR type grid, each interlobe may have a different number of nodes and their distribution on the rotor profile may change. Therefore, it is necessary to make a coordinate transformation for the full profile span.

If the boundary points are represented in the index notation with respect to the physical coordinate system as  $r_{i,j}(x, y)$ . The points on the inner boundary have index  $j=0$  i.e.  $r_{i,j=0}(x, y)$  and the points

on the outer boundary are  $r_{i,j=1}(x, y)$ . In addition, an outer circle with diameter larger than the rotor outer diameter is discretised using the nomenclature  $r_{i,j'=1}(x, y)$ , as shown in Figure 6.

The node distribution starts at the bottom CUSP which has index  $i=0$ . Based on the equidistant spacing, the distribution of the outer boundary is defined as,

$$|r_{i,j=1}(x, y)| = |r_{i-1,j=1}(x, y)| + S_i i \quad (1)$$

$S_i = \frac{S_1}{I}$  is the increment in spacing per node.  $S_1$  is the length of the boundary and  $I$  is the number of nodes on the rack and casing which can be set independently. The transformation from the physical region  $X^2$  onto a computational domain  $\Xi^2$  is such that the outer circular boundary becomes a straight line along the  $\xi$  coordinate. The transformation is described by equations (2a, 2b and 2c) below. It is to be noted that in the forward transformation, the rotor profile is defined with a high density array while in the reverse transform, the inner boundary is discretised with the same number of points as the outer boundary.

Outer boundary

$$\xi_{i,j=1}(x, y) = \tan^{-1} \left( \frac{y_{i,j=1}}{x_{i,j=1}} \right) \quad (2a)$$

$$\eta_{i,j=1}(x, y) = r_o - \sqrt{x_{i,j=1}^2 + y_{i,j=1}^2}$$

Outer circle

$$\xi_{i,j'=1}(x, y) = \tan^{-1} \left( \frac{y_{i,j'=1}}{x_{i,j'=1}} \right) \quad (2b)$$

$$\eta_{i,j'=1}(x, y) = r_o - r_{oc}$$

Inner boundary

$$\xi_{i,j=0}(x, y) = \tan^{-1} \left( \frac{y_{i,j=0}}{x_{i,j=0}} \right) \quad (2c)$$

$$\eta_{i,j=0}(x, y) = r_o - \sqrt{x_{i,j=0}^2 + y_{i,j=0}^2}$$

Where,  $r_o$  is the radius of the rotor and  $r_{oc}$  is radius of outer circle.

The reverse transformation from computational domain to physical region is required only for the rotor profile in order to obtain the distribution of the inner boundary nodes on the rotor in the physical domain.

This reverse transformation is represented by the following equation (3).

$$x_{i,j=0}(\xi, \eta) = abs \left[ r_o - \eta_{i,j=0}(x, y) \right] \cos \left[ \xi_{i,j=0}(x, y) \right] \quad (3)$$

$$y_{i,j=0}(\xi, \eta) = \text{abs} \left[ r_0 - \eta_{i,j=0}(x, y) \right] \sin \left[ \xi_{i,j=0}(x, y) \right]$$

Figure 8 shows the distribution obtained after the reverse transformation. Here the distribution on the inner boundary is obtained using equidistant distribution.

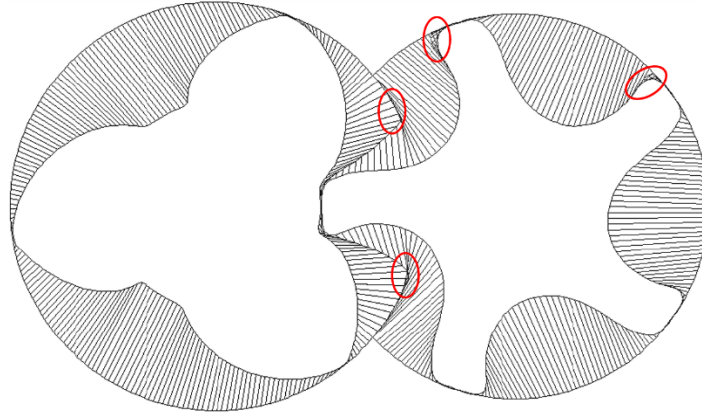


Figure 8 Reverse transformation of full rotor region to physical domain

As shown in Figure 8, the difference in rotor curvatures may result in a significant number of irregularities and crossing of the distribution lines. However, at the same time a conformal interface has been achieved between the two O blocks which renders the need for merging nodes on the CUSP point. This is because grid points on the outer boundary are stationary and both CUSPs have the same index  $i$  in all the cross sections forming naturally a straight CUSP line. However it is necessary to regularise the distribution on the inner boundary in the computational domain before the reverse transformation is carried out in order to ensure that the final distribution of the nodes on the rotor surface is regular.

## 2.2 Regularisation approach using analytical control function

A conformal interface between the two rotor blocks requires nodes on the dividing rack curve to correspond for both O grids. This imposes a constraint on the distribution of the outer boundary which should remain unchanged in the computational space. To achieve that and regularise the distribution on the inner boundary, an additional outer circle was introduced with a certain offset from the casing circle as shown in Figure 6. This outer circle is discretised with the same number of nodes as the outer boundary. Each node on this outer circle is now treated as a controller of the corresponding node to be placed on the inner boundary as shown in Figure 9a. When the control node on the outer circle is made to move to the left in computational space, then the intersection point with the rotor profile will move to the right like an action of a lever. The magnitude of the leverage will be controlled by the difference in diameter of the outer computational circle from the outer boundary and the depth between the outer boundary (rack point) and the inner boundary (rotor profile point). Thus independent control on each point on the rotor profile is achieved by controlling the node movement on the outer computational circle. A function needs to be formulated which will provide control on the spacing of the nodes on the

outer circle and also control the location of the focus point to which these points will attract or repel. Such a control is achieved by a skewed sine function defined in equation 4.

$$f(t) = A_{sk} - abs \left\{ A_{sk} \sin \left[ 2 \pi n_{sk} \frac{t}{t_i} - \sigma_{sk} abs \left( \sin \left( 2 \pi n_{sk} \frac{t}{t_i} \right) \right) \right] \right\} \quad (4)$$

Points are represented by the index  $i$ . Skewness value controls the location where the function will have zero value while the amplitude controls the magnitude of the function at a given point. The number of cycles of the function correspond to the number of lobes on the rotor.

Figure 9a shows the regularised distribution obtained on the main and gate rotors in the computational space. In the interlobe space where the outer boundary is represented by the rack curve, the sine function is made to work only between the CUSP points. The casing points on the outer boundary are aligned with the starting and ending points in two CUSPs to provide smooth distribution. Figure 9b shows the distribution in the physical domain obtained by reverse transformation where the required properties of the conformal interface are achieved in each 2D cross section using the skewed sine function.

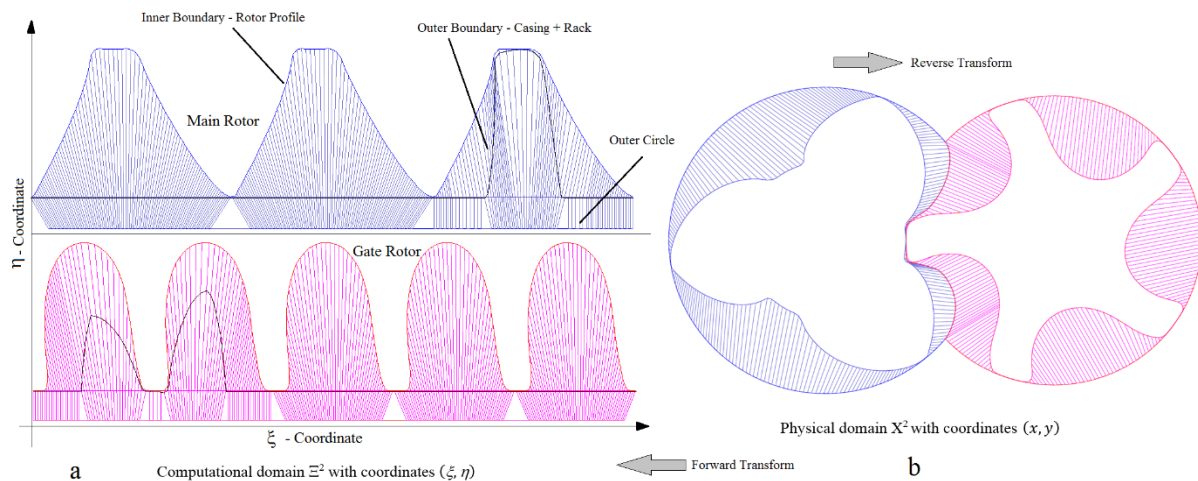


Figure 9 CR distribution obtained with skewed sine function – a) Computational space, b) Physical space

An example of the CR mesh with the conformal interface produced using skewed sine adaptation of the rotor distribution is shown in Figure 10 on “N” profile rotors with 3 male rotor lobes and the gate rotor of 5 lobes. These rotors have deep lobes with small radii at the rotor tip and the convex trailing side of the female rotor lobe. Because of these features a relatively high skewness and amplitude factors are required to achieve regular distribution in 2D cross sections. Figure 10 shows details of the cross section with the interface regions and the 3D grid of the helical rotors.

The control parameters listed in Table 2 were used for the grid generation. The node counts have been selected so as to get reasonable size and resolution of the grid and rotor profile. Control parameters in Table 2 were started with 0 such that skewness and amplitude is inactive and result is a non-regular

distribution (Figure 8). Final values reported in Table 2 were obtained by gradual increment such that distribution becomes regular (Figure 9b). Cell quality has not been considered at this stage.

Table 2 Control parameters for sample case using skewed sine function

Total number of circumferential nodes			250		
Circumferential nodes in the interlobe			65		
Radial Nodes			8		
Angular divisions per interlobe angle			50		
Skewed sine function:	Main Rotor	Skewness	+0.2	Amplitude	0.25
	Gate Rotor	Skewness	-0.5	Amplitude	0.24

However, generation of a 3D mesh showed highly skewed cells on the surface of the male rotor occurring in the place of an abrupt change in the rack curve shape between two consecutive cross sections, as shown in Figure 11. This difficulty was not observed for the rotors with straight lobes because all cross sections in such rotors are identical but a jump in the cell shape was noticed. As such, the method of using a skewed sine function for regularisation of rotor profile distribution has been successful for generation of conformal fully hexahedral grids for rotors with straight lobes, but was not successful for screw rotors with helical lobes.

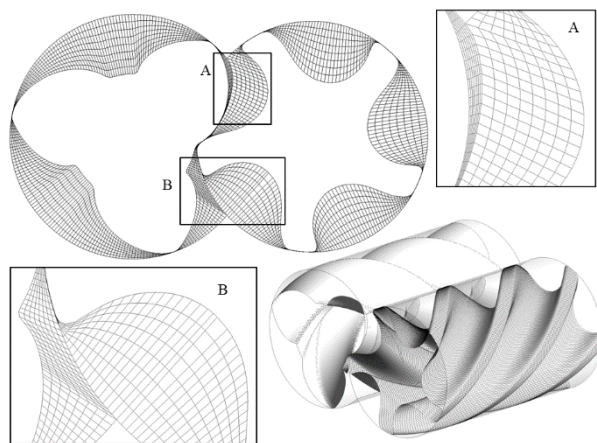


Figure 10 Conformal grid regularised by use of skewed sine function

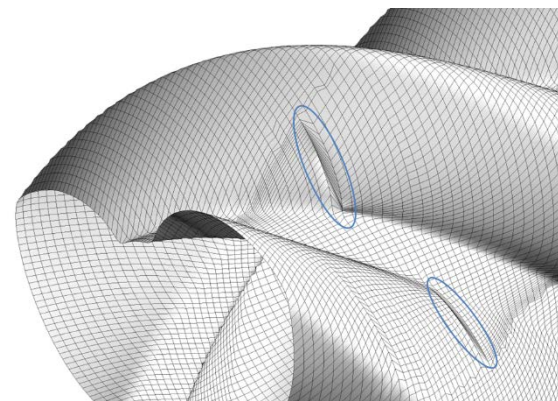


Figure 11 Degenerated faces on the rotor surface in 3D grids

### 2.3 Regularisation approach using background blocking technique

The second approach formulated here for distribution of nodes on the rotor profile is based on the principle of blocking used in multi block grid generation techniques (*Thompson, Soni and Weatherill,*

1999 [24], *Eiseman et al.*, 1994 [3]). The procedure is used to distribute nodes on the inner boundary (rotors) of the new CR type mesh by use of background blocks generated from the RC type grid. Apart of regularisation of distribution, this approach can be used for an independent refinement of the grid in the interlobe region in order to improve the mesh quality in the interlobe leakage gaps.

A skewed sine function for regularisation of the rotor profile distribution independently regularised each 2D cross section. This produced degenerated cells in the 3D mesh. In order to achieve regular 3D mesh with helical rotors, distribution on the rotor profile requires reference to adjacent cross sections. The distribution of points on the rotor surface in RC grid type, which is directed from the rotor profile to the outer boundary generates a very good quality rotor surface mesh. This feature of the RC grid type makes this distribution suitable for background blocking in the new CR type distribution on the rotor profile.

### 2.3.1 Generating background blocks

Background blocks are produced by equidistant distribution in the RC grid type on the outer computational circle. The outer circle will normally have diameter of the rotor bores as shown in Figure 12.

Background blocks are generated using following steps:

1. Nodes on the rotor profile in each interlobe are distributed, using equidistant distribution. If required adaptation described in (*Kovačević et al.*, 2002) [9] can be applied.
2. The distribution on the outer circle is based on regularised arc-length as described in *Kovačević et al.*, 2002 [9].
3. This is used as background distribution block as shown in Figure 12.

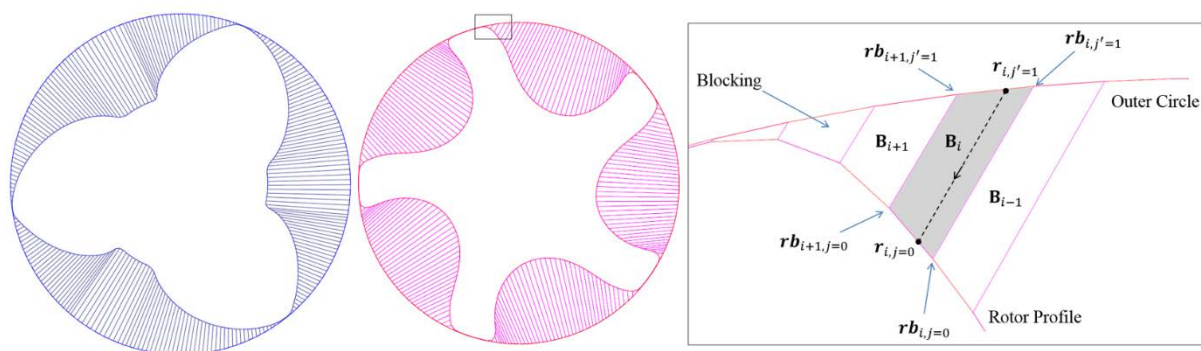


Figure 12 Background blocking for the main and gate rotors and projection function

The advantages of generating such blocks are:

- The blocks do not have to be as refined as the final grid.
- The blocks can be used as reference for refinement in any required region.
- The blocks have to be calculated only once and simply rotated for other rotor positions.

### 2.3.2 Application of background blocking

As shown in Figure 6 the points distributed on boundaries are represented in the index notation with respect to the physical coordinate system as  $\mathbf{r}_{i,j}(x, y)$ . Points on the inner boundary (rotor profile) are  $\mathbf{r}_{i,j=0}(x, y)$ , points on the outer boundary which consists of casing and rack curve are  $\mathbf{r}_{i,j=1}(x, y)$  and the points distributed on the outer circle are  $\mathbf{r}_{i,j'=1}(x, y)$ .

Each of the background blocks is identified by its index  $\mathbf{B}_i$ . The background block points on the inner boundary of the blocks are  $\mathbf{rb}_{i,j=0}(x, y)$  and the background block points on the outer full circle are  $\mathbf{rb}_{i,j'=1}(x, y)$  as shown in Figure 12.

Starting from the bottom CUSP, nodes are distributed on the outer circle corresponding to the rack part with required number of points  $i_{rack}$  as shown in Figure 13. The remaining nodes are distributed on the outer circle covering the casing part with required number of points  $i_{casing}$ . Factors  $i_{rack}$  and  $i_{casing}$  can be independently selected for the main and the gate rotor or they can be set such that the sum  $i_{rack} + i_{casing}$  is maintained. Increasing the number of points in the interlobe between two CUSPS  $i_{rack}$  will coarsen the casing part and refine the rack part of the outer boundary. At this stage  $\mathbf{rb}_{i,j=0}(x, y)$ ,  $\mathbf{rb}_{i,j'=1}(x, y)$  and  $\mathbf{r}_{i,j'=1}(x, y)$  are known and it is required to calculate the position of the new point on the rotor  $\mathbf{r}_{i,j=0}(x, y)$  as shown in Figure 12. This node distribution is based on equidistant spacing

$$|\mathbf{r}_{i,j'=1}(x, y)| = |\mathbf{r}_{i-1,j'=1}(x, y)| + S_i i \quad (5)$$

where  $S_i = \frac{S_1}{I}$ ,  $S_1 = |\mathbf{r}_{i,j'=1}(x, y) - \mathbf{r}_{i=0,j'=1}(x, y)|$ . Since the calculation of new point using equation (5) is separate for the rack part and for the casing part, value of  $I = i_{rack}$  on the rack and  $I = i_{casing}$  on the casing. The process is managed by a scanning function which has the information of the background blocking. Starting from the bottom CUSP, the scanning function traces each node  $\mathbf{r}_{i,j'=1}(x, y)$  and identifies the block  $\mathbf{B}_i$  to which this node belongs. There can be a situation when a single block contains multiple nodes of the distribution on the outer boundary or blocks which contain no nodes. This is because the distribution on the outer boundary can be refined either in the rack part or in the casing part and be different than the blocking. Once the nodes associated with each block are found by the scanning function, an arc-length based projection is used to determine the nodes  $\mathbf{r}_{i,j=0}(x, y)$  to be placed on the inner boundary - rotor profile. At the same time constraint is imposed on the node placement that they have to be bound in the same block  $\mathbf{B}_i$  as that of the outer circle nodes  $\mathbf{r}_{i,j'=1}(x, y)$ .

Figure 12 shows the projection of  $\mathbf{r}_{i,j'=1}(x, y)$  on the inner boundary of the block which gives corresponding  $\mathbf{r}_{i,j=0}(x, y)$  based on the arc-length factor given by equation (6).

$$\mathbf{r}_{i,j=0}(x,y) = \mathbf{rb}_{i,j=0}(x,y) + \left( \mathbf{rb}_{i+1,j=0}(x,y) - \mathbf{rb}_{i,j=0}(x,y) \right) \frac{S_i}{S_I}$$

$$S_i = \mathbf{r}_{i,j'=1}(x,y) - \mathbf{rb}_{i,j'=1}(x,y)$$

$$S_I = \mathbf{rb}_{i+1,j'=1}(x,y) - \mathbf{rb}_{i,j'=1}(x,y)$$
(6)

The calculated position of inner boundary nodes  $\mathbf{r}_{i,j=0}(x,y)$  ensure that they are placed on the original rotor profile. Regularised distribution is then superimposed onto the outer boundary - rack curve by finding the intersection points of the distribution line and the rack curve. These intersection points define the new point distribution  $\mathbf{r}_{i,j=1}(x,y)$  on the rack curve as shown in Figure 13.

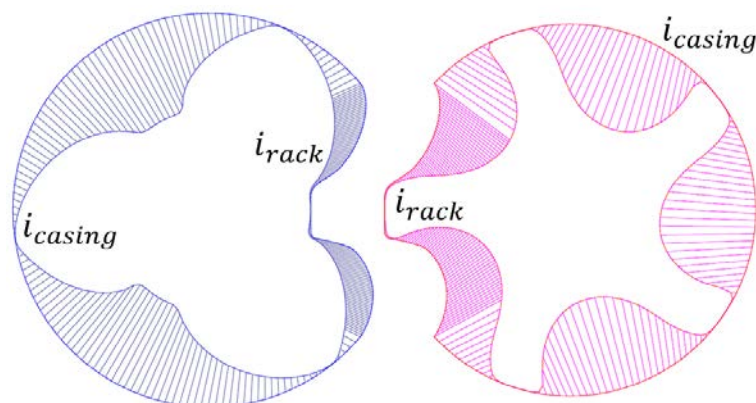


Figure 13 Refinement in the rack segment and superimposition of rack curve

The blocks are different on the male and the female rotor side and accordingly the intersection points obtained on the common rack on the two O blocks are initially different. This results in a non-conformal interface between the two rotor blocks but gives the grid an important capability of refinement in the interlobe region. This flow region contains interlobe gaps which are a big factor in the performance of the machine and therefore accurate capturing of the rotor profile in the leakage gaps has a strong influence on the solution of the leakage flow calculation.

Additionally, it is possible to constrain the node distribution on the rack segment of the outer boundary to be same for both O blocks of the main and gate rotor and therefore achieve a one to one conformal interface as shown in Figure 14. Thus a non-conformal interface can be replaced by the conformal interface and a single domain structure for the rotor mesh can be constructed.

### 2.3.3 Regularised grid with background blocking

The same example shown in section 2.2 which explained the skewed sine function is used here to demonstrate the quality of the mesh obtained by the background blocking. The grid parameter values listed in Table 3 were used for the grid generation. The node counts have been selected so as to get reasonable size and resolution of the grid and rotor profile. No special control parameters are required with background blocking as in the case of a skewed sine function.

Table 3 Grid parameters for sample case using background blocking.

Blocks per interlobe	Main Rotor	80
	Gate Rotor	50
Total number of circumferential nodes		250
Circumferential nodes in the interlobe		75
Radial Nodes		8
Angular divisions per interlobe angle		50

Figure 14 shows the grid of the helically lobed screw compressor rotors generated by use of background blocking. The 2D mesh in a typical cross section with enlarged interface regions and the 3D grid of the rotors shows big improvements when compared with the previously generated meshes. The mesh in the cross sections shows all quadrilateral cells with a possibility for independently setting the number of nodes in the interlobe region. Figure 15 shows the 3D rotor grid on the inner and outer boundary obtained by the use of background blocking. The skewed sine function had resulted in degenerated faces on the surface mesh of these rotors as shown in Figure 11. However with the background blocking approach, the 3D grid is fully hexahedral and both the main and the gate rotor surfaces are smoothly captured. Some small non-aligned node movements are observed at the transition point from the interlobe region to the casing region on the rotors surface. However, these still result in all regular cells which does not show any issues in CFD calculations. The numerical grid on the casing surface is of the highest quality with regular quadrilateral cells. The surface mesh in the interlobe interface has axial grid lines with large jumps, which are cyclically repeated in every set of cross sections near the top and bottom CUSP's. These are caused by the abrupt movement of the rack line but as they occur on the surface of the interface these do not result in any irregular cells. In all the cross sections, the index of the top and bottom CUSP points is the same and hence a straight line is obtained in the axial direction which captures the blow-hole area accurately.

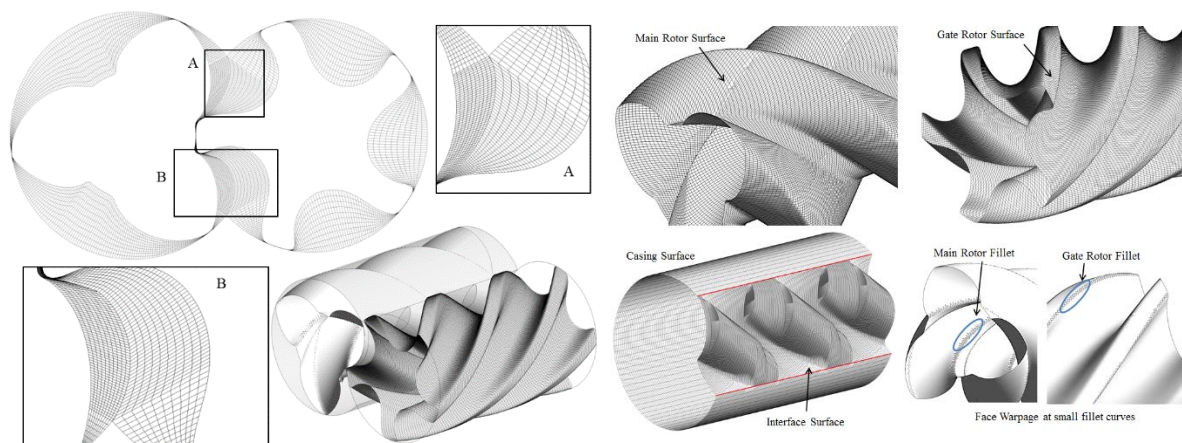


Figure 14 Grid generated with background blocking in screw compressor rotor      Figure 15 Surface mesh on the rotor, casing and the rack interface

The CR grid type is characterised by the stationary casing mesh and sliding mesh on the rotors. Due to this sliding action some face warping of the cells are noticeable at the root of the main rotor and at the tip of the gate rotor where normally small fillets are introduced in the rotor profile, as shown in Figure 15. This is reported also in *Vande Voorde (2005) [27]* and is a feature of CR type grid which does not happen in the RC grid type where the nodes rotate together with rotors. The effect of this face warping can be reduced by increasing number of points on the grid and is assessed further in the section 3 of this paper.

## 2.4 Examples

The examples of interlobe refinement and the conformal interface between the blocks are shown here to demonstrate capability of the new method for generating single domain numerical mesh for screw machines.

### 2.4.1 Example of the grid with interlobe refinement

Figure 16 shows an example of successively increased refinement in the interlobe region. The sum of  $i_{rack} + i_{casing}$  is maintained constant while the number of points on the rack are increased. This has the effect of coarsening the casing part and refining the rack part as the  $i_{rack}$  is increased from 75 to 200, but the total mesh size remains constant. Even with large differences between the number of nodes on the casing and the number of nodes on the rack segment, a rotor surface is smooth and well captured. This is because the background blocking ensures that the nodes are always placed within the constraints guided by the rotor profile. With higher number of  $i_{rack}$  nodes, the rotor curvature in the interlobe region is captured more accurately and this will result in better prediction of the interlobe leakage flow. A large change in cell volumes occurs at the transition from the rack to the casing region which could be mitigated by the increase in the cell size or a gradual redistribution of the casing nodes towards the CUSP regions to obtain as smooth transition as possible.

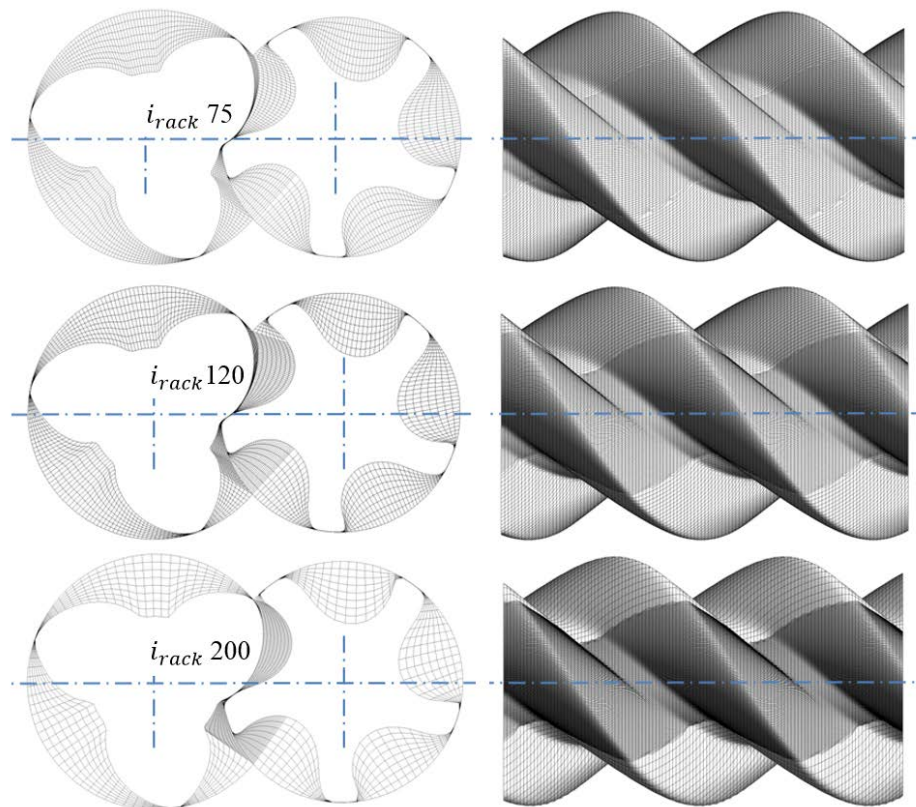


Figure 16 Examples of grids with interlobe refinement

#### 2.4.2 Example of the grid with conformal interface

Figure 17 shows an example of the grid in cross section with the conformal interface between the two O blocks which features node to node connection. The distribution was generated first on the rack part of the gate rotor and maintained identical on the main rotor block thus achieving a conformal interface the interlobe region.

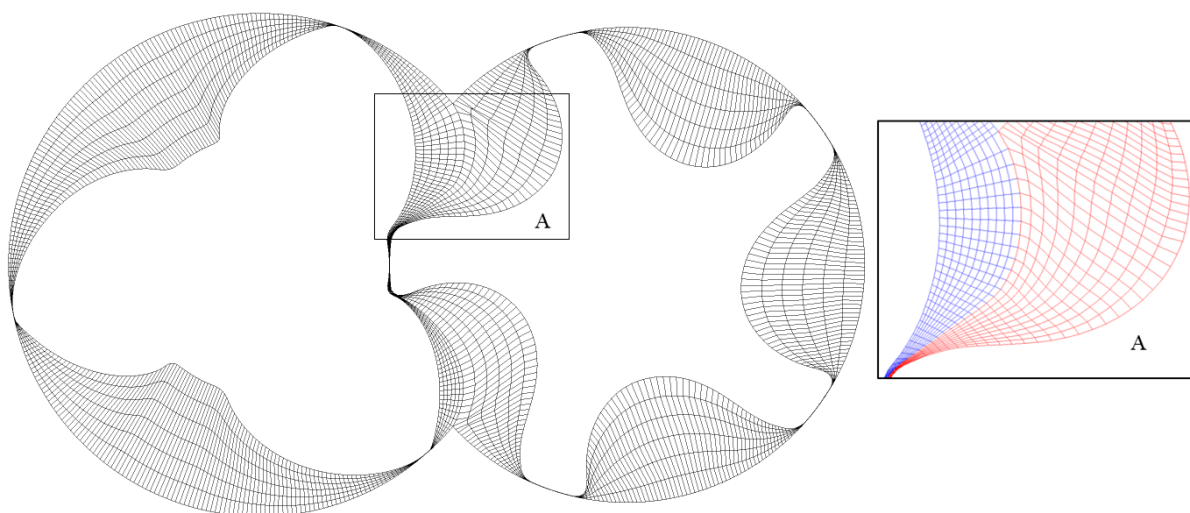


Figure 17 Example of the grid with a single mesh domain for both rotors

In the process of generating a 3D mesh for solving the fluid flow around these rotors, the corresponding nodes in the interface are collapsed in the single node and a single domain cell structure is produced.

### 3 Evaluation of the cell quality of the CR type grids

Numerical grids used for calculation of fluid flow by Computational Fluid Dynamics (CFD) need to be acceptable by the flow solver, have all cells regular and should capture the geometry at boundaries as accurately as possible. If a large numbers of cells are with poor quality then the error induced in numerical calculations is large resulting in inaccurate or false predictions from the CFD models. At the same time large number of poor quality cells can lead to solver instability and convergence issues particularly at higher operating pressure ratio. Moreover, even if the calculation is possible, large number of poor quality cells will increase calculation time to achieve desired convergence criteria. Some of the important quality criteria for finite volume numerical methods are orthogonality, skewness, aspect ratio and warpage of cells. These are considered below for evaluation of the CR type grids.

For comparison, two grid types are considered, as follows:

Grid A – RC grid type which has been well validated as acceptable for flow solutions using variety of CFD solvers including ANSYS CFX solver (*Kovačević et al., 2007*) [11].

Grid B – the newly formulated algebraic CR grid type produced by background blocking regularization.

The size of the mesh in terms of the node count and spacing in the circumferential, radial and axial directions is same for both grids. The commercial ICEM CFD tool from ANSYS has been used for the calculation of quality factors and plotting of selected cells.

#### 3.1 Orthogonality

The orthogonality is a cell quality defined as the cosine of the angle between the vector normal to the cell face and the vector from the cell centroid to the centroid of the adjacent cell or the vector from the cell centroid to its face centroid. The smaller of the two values is selected. A value of 1 represents a perfect hexahedral cube and a value of 0 is a fully degenerated hexahedron.

Grid A showed an average orthogonality of 0.63, while Grid B showed an improved average orthogonality of 0.82. At the minimum quality level, Grid A has about 50 cells with orthogonal quality less than 0.05 whereas in case of Grid B it is only in 6 cells. From Figure 18a, Grid A has about 43% cells with orthogonal quality higher than 0.7 while Grid B has about 88% cells with orthogonal quality higher than 0.7. An orthogonal quality factor greater than 0.3 is recommended by ANSYS CFX solver and is in the same range for most of the flow solvers. An improvement in orthogonal quality in Grid B is because the grid lines in the axial direction run normal to the cross section faces as opposed to those running along the helix of the rotors in the case of Grid A.

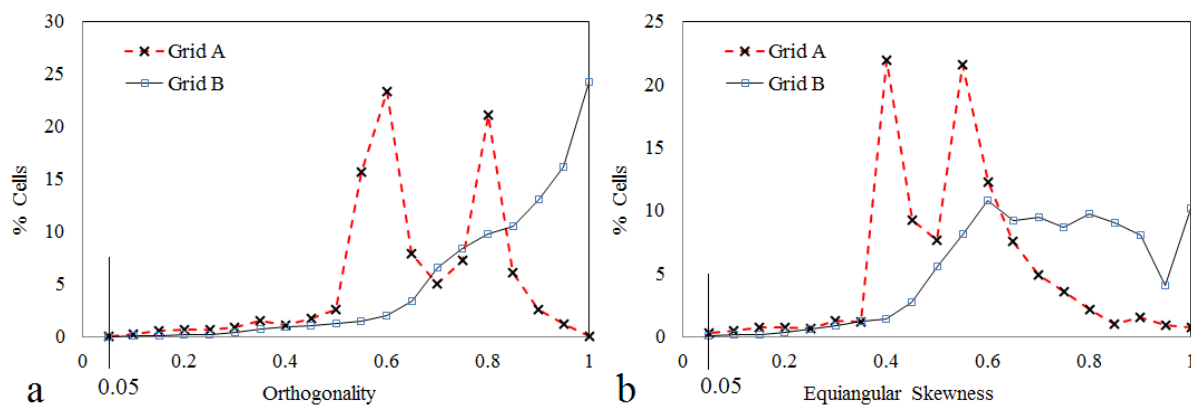


Figure 18 Comparison of Grid A and Grid B - % cells vs Quality factor

### 3.2 Equiangular Skewness

Equiangular Skewness is calculated as the deviation of the cell with respect to a perfect cubic hexahedron as given by equation (7). A value of 1 represents a perfect hexahedral cube while a value of 0 represents a fully degenerated hexahedron.

$$Equiangular\ Skewness = 1.0 - \text{Max} \left( \frac{(Q_{max} - Q_e)}{(180 - Q_e)}, \frac{(Q_e - Q_{min})}{Q_e} \right) \quad (7)$$

Where,  $Q_{max}$  and  $Q_{min}$  = largest and smallest angle in the element

$Q_e = 90^\circ$ , angle of an equiangular element

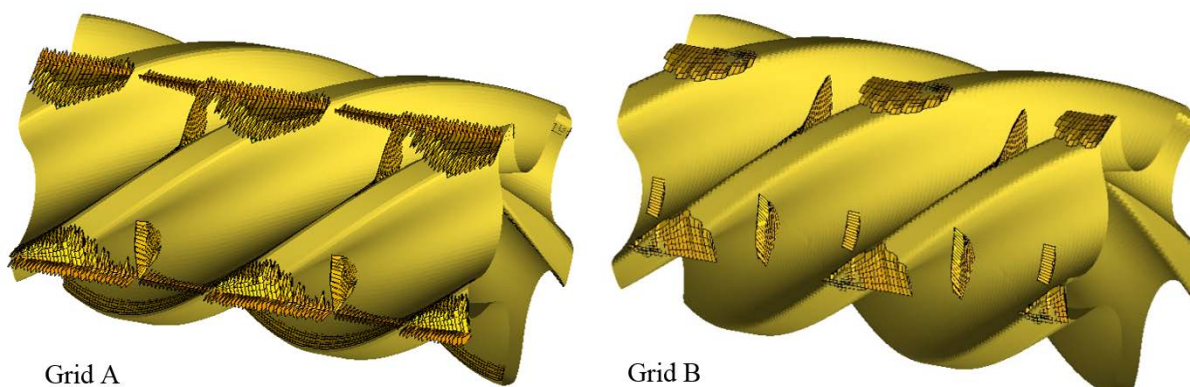


Figure 19 Comparison of cells with Equiangular Skewness factor < 0.15

Grid A showed an average equiangular skewness of 0.49 while Grid B showed an improved average equiangular skewness of 0.66. At the minimum quality level, Grid A has about 1694 cells with equiangular skewness less than 0.05 whereas in case of Grid B it is only in 232 cells with 0.01 as the lowest quality. Grid A has a minimum equiangular skewness of zero in some cells because of the nodes merged at the top and bottom CUSP's as shown in Figure 3. From Figure 18b, Grid A has about 1.4%

cells with equiangular skewness lower than 0.15 while Grid B has about 0.35% cells with equiangular skewness lower than 0.15. The location of cells with the equiangular skewness  $< 0.15$  is shown graphically in Figure 19. The Grid B of CR type shows great improvement in skewness compared to the original mesh. The highest degeneration of cells is on the interface in the interlobe region which indicates that it may be possible to improve this further by smoothing the interface curve.

### 3.3 Aspect Ratio

The Aspect Ratio is an indicator of the degree of stretching on the cells. For an individual hexahedral cell it is defined as the ratio of its maximum face area to its minimum face area. For the entire grid the largest ratio is considered as the maximum aspect ratio. In Grid A the aspect ratio was found to be 230 in the main rotor and 280 in the gate rotor in less than 0.1% cells. In Grid B the aspect ratio was found to be 443 in the main rotor and 348 in the gate rotor in less than 0.1% cells. Maximum Aspect ratio recommended by ANSYS CFX solver is less than 100. But for double precision it can be as high as 1000 in limited number of cells. Cell locations with aspect ratio exceeding 200 are represented graphically in Figure 20 which clearly shows that these high aspect ratio cells are present in the radial and interlobe leakage gaps.

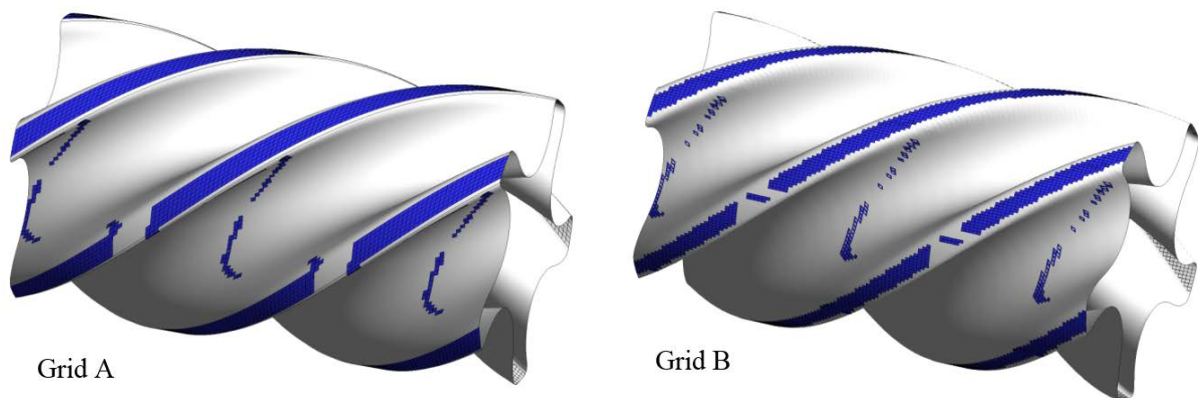


Figure 20 Comparison of regions with aspect ratio  $> 200$

### 3.4 Face warp angle

The warpage factor or the face warp angle indicates the level of cell distortion. The nodes which form a cell face are expected to be in a same plane in which case these will produce a cell with small warping. The maximum warp of a hexahedron is defined as the maximum warp of its faces. A value of  $0^\circ$  represents a perfect hexahedron and a value of  $90^\circ$  is a fully degenerated hexahedron. Grid A showed an average Warp angle factor of  $4.9^\circ$  while Grid B showed an increase in the average Warp angle to  $7.0^\circ$ . Figure 21 highlights the cells in the main rotor domain with Max Warp angle greater than  $50^\circ$ . In Grid B, the cells with the higher warp angle are at the root fillet of the profile since the grid lines in the axial direction do not align with the helix of the rotor. This has decreased the global Warp angle quality

of the cells as compared with those in Grid A. In Grid A, 96% of cells have a good Warp angle in the range of  $0^\circ - 10^\circ$  while in Grid B this number has reduced to 75%.

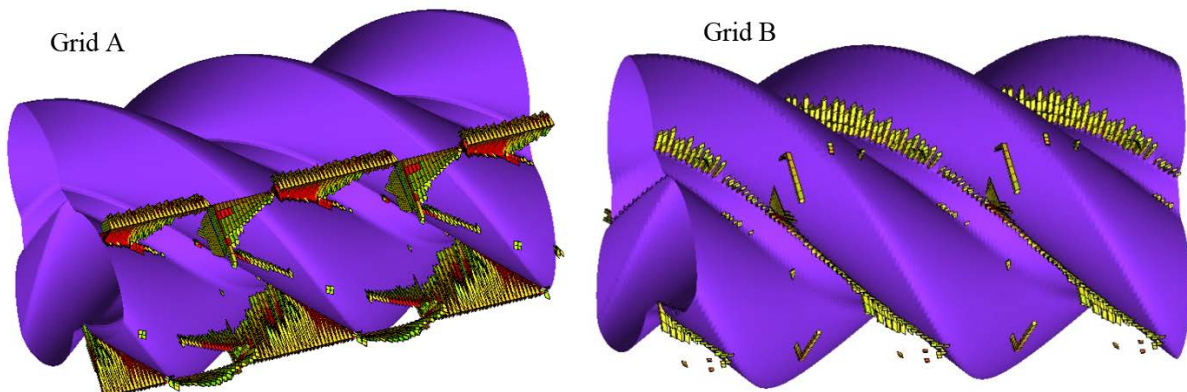


Figure 21 Comparison of cells with MaxWarp factor  $> 50$

From the analysis of above quality parameters it can be concluded that the CR grid type have acceptable quality for the solver. The cell orthogonality and equiangular skewness have improved significantly, but the maximum warp angle has increased for the CR type grid when compared to RC type grid. The aspect ratio was maintained in the same range in both grid types.

#### 4 Conclusions

Computational fluid dynamics of twin screw machines requires special attention in the generation of a computational grid that needs to represent the highly deforming working chamber in such machines. In practise two algorithms are available namely, an algebraic decomposition method from *Kovačević et al* (2002) [9] and a differential decomposition method from *Vande Voorde et al* (2005) [26]. Algebraic methods produce RC type mesh which rotates with rotors and take very little time measured in minutes to produce full mesh while the differential methods produce CR type mesh which is stationary on the casing and slides on the rotors and take very long time measured in tens of hours to obtain converged mesh. In this paper an algebraic method is developed in order to improve speed and accuracy of the CFD solution and enable use of variety of CFD solvers for analysis of screw machines. A new algebraic boundary distribution of CR type has been implemented to generate a single domain rotor grid.

This paper presented the implementation and grid characteristics of the new method.

- Using a boundary distribution governed from the casing boundary to the rotor boundary (CR type grids) and the regularisation functions, it was possible to achieve desirable characteristics in the twin screw rotor domain;
  - Firstly, the independent refinement of the numerical mesh in the interlobe leakage region thereby providing better accuracy in representation of rotor curvature in the gaps. In this respect, it was found that grid generation was more robust with a non-conformal interface between the rotor grid blocks.

- Secondly, a highly significant achievement is a single domain structured grid for the rotors which eliminates a non-conformal interface between the two rotor domains, while still maintaining the fully hexahedral cell topology.
- Regularisation based on analytical function was suitable for non-helical rotors but failed for helical screw rotors due to degeneration of the rotor surface mesh.
- Regularisation based on background blocking approach was highly successful, easy to implement and robust.
- The speed of calculation of the numerical mesh is very short allowing the full moderate size mesh of around 1 million cells to be generated within few minutes in comparison with differential methods which use more than 10 hours to generate similar mesh.
- With this CR grid approach, an improvement in the global orthogonality and skewness of the cells was measured in a 3/5 helical screw rotor mesh.
- Aspect ratio did not show a significant difference between the RC type and CR type grid structures.
- With CR type structure, there was a decrement in the face warp quality at tip of the rotors which will need attention in further work.

This development allowed the use of numerical mesh generated by algebraic grid generation with variety of CFD solvers including popular ones like ANSYS CFX, ANSYS Fluent, CD Adapco STAR-CCM+ and Simerics PD.

## References

- [1] Chawner J. R., Anderson D. A., 1991. Development of an Algebraic Grid Generation Method with Orthogonality and Clustering Control, Conference on Numerical Grid Generation in CFD and Related Fields at Barcelona, 107.
- [2] Eiseman P. R., 1987. Adaptive grid generation. *Comput. Methods. Appl. Mech. Eng.* 64, 321-376.
- [3] Eiseman P.R., Hauser J., Thompson J.F., Weatherill N.P., (Ed.), 1994. Numerical Grid Generation in Computational Field Simulation and Related Fields, Proceedings of the 4th International Conference, Pineridge Press, Swansea, Wales, UK.
- [4] Farrashkhalvat M., Miles P. J., 2003. Basic structured grid generation with an introduction to unstructured grid generation. BH publication Oxford. ISBN 0 7506 5058 3.
- [5] Ferziger J. H. and Perić M., 1996. *Computational Methods for Fluid Dynamics*, ISBN 978-3-540-42074-3, Springer, Berlin, Germany.
- [6] Gordon W.J., Hall C.A., 1973. Construction of Curvilinear Coordinate Systems and Applications to Mesh Generation, *Int. J. Numer. Meth. Engineering*, Vol.7, 461-477.

- [7] Kim J. H., Thompson J.F, 1990. 3-Dimensional Adaptive Grid generation on a Composite-Bloch Grid, *AIAA Journal*, Vol.28, Part.3, 470-477.
- [8] Kovačević A., Stošić N., Smith I. K., 2000. Grid Aspects of Screw Compressor Flow Calculations, *ASME Congress*, Orlando FL, Vol. 40, pp. 83.
- [9] Kovačević A., 2002. Three-Dimensional Numerical Analysis for Flow Prediction in Positive Displacement Screw Machines, Ph.D. Thesis, School of Engineering and Mathematical Sciences, City University London.
- [10] Kovačević A., 2005. Boundary Adaptation in Grid Generation for CFD Analysis of Screw Compressors, *Int. J. Numer. Methods Eng.*, Vol. 64: 401-426.
- [11] Kovačević A., Stošić N. and Smith I. K., 2007. Screw compressors - Three dimensional computational fluid dynamics and solid fluid interaction, ISBN 3-540-36302-5, Springer-Verlag Berlin Heidelberg New York.
- [12] Kovačević A. and Rane S., 2013. 3D CFD analysis of a twin screw expander, 8th International conference on compressors and their systems, London, p. 417.
- [13] Papes, I., Degroote, J., Vierendeels, J., 2014. 3D CFD analysis of a twin screw expander for small scale ORC systems. *Proceedings of the 11th World Congress on Computational Mechanics*. pp. 7207–7217.
- [14] Rane S., Kovačević A., Stošić N. and Kethidi M., 2013. Grid Deformation Strategies for CFD Analysis of Screw Compressors, *Int Journal of Refrigeration*, 36, 7, p. 1883-1893.
- [15] Rane S., Kovačević A., Stošić N. and Kethidi M., 2014. Deforming grid generation and CFD analysis of variable geometry screw compressors, *Computers and Fluids*, 99, p. 124–141.
- [16] Riemsdagh K., Vierendeels J., Dick E., 2000. An arbitrary Lagrangian-Eulerian finite-volume method for the simulation of rotary displacement pump flow. *Applied Numerical Mathematics*, 32:419-433.
- [17] Samareh A. J., Smith R.E., 1992. A Practical Approach to Algebraic Grid Adaptation, *Computers Mathematical Applications*, Vol.24, No.5/6, 69-81.
- [18] Shih T. I. P., Bailey R. T., Ngoyen H. L., Roelke R. J., 1991. Algebraic Grid Generation for Complex Geometries, *International Journal for Numerical Methods in Fluids*, Vol. 13, 1-31.
- [19] Sorenson R. L., Steger J. L., 1977. Simplified clustering of nonorthogonal grids generated by elliptic partial differential equations. Ames research centre, Moffett field, California, NASA Technical Memorandum 73252.
- [20] Soni B.K, 1992. Grid Generation for Internal Flow Configurations, *Computers Mathematical Applications*, Vol.24, No.5/6, 191-201.
- [21] Steger J. L., Sorenson R. L., 1979. Automatic mesh-point clustering near a boundary in grid generation with elliptic partial differential equations. *J. Comput. Phys.* 33, 405-410.

- [22] Stošić N, Smith I.K, Zagorac S, 1996. CFD Studies of Flow in Screw and Scroll Compressors. Proc. Int. Compressor Conf. at Purdue. Paper 1103.
- [23] Thompson J. F., Thames F. C., Mastin C. W., 1974. Automatic Numerical Generation of Body-Fitted curvilinear coordinate system for field containing any number of arbitrary two-dimensional bodies. J. Comput. Phys., vol. 15, pp. 299-319.
- [24] Thompson J. F, Soni B and Weatherill N. P, 1999. Handbook of Grid Generation, CRC Press.
- [25] Vande Voorde J., Vierendeels J., Dick E., 2004. A Grid Generator for flow calculations in Rotary Volumetric Compressors, European Congress on Computational Methods in Applied Sciences and Engineering.
- [26] Vande Voorde J., Vierendeels J., 2005. A grid manipulation algorithm for ALE calculations in screw compressors. 17th AIAA Computational Fluid Dynamics Conference, Canada, AIAA 2005-4701.
- [27] Vande Voorde J., 2005. Numerical flow calculations in rotary positive-displacement machines. PhD Thesis. Ghent University.
- [28] Winslow A., 1966. Numerical solution of the quasilinear poisson equation in a nonuniform triangle mesh. J. Comput. Physics, 1:149-172.
- [29] Kovacevic A., and Rane S., 2017. Algebraic Generation of Single Domain Computational Grid for Twin Screw Machines Part II – Validation. *Advances in Engineering Software*. Under review.